The Astrophysical Journal, 730:112 (12pp), 2011 April 1 doi:10.1088/0004-637X/730/2/112

THE M33 GLOBULAR CLUSTER SYSTEM WITH PAndAS DATA: THE LAST OUTER HALO CLUSTER?

Robert Cockcroft[1], William E. Harris[1], Annette M. N. Ferguson[2], Avon Huxor[3], Rodrigo Ibata[4], Mike J. Irwin[5], Alan W. McConnachie[6], Kristin A. Woodley[7], Scott C. Chapman[5], Geraint F. Lewis[8], and Thomas H. Puzia[9]
[1] Department of Physics and Astronomy, McMaster University, Hamilton, Ontario L8S 4M1, Canada; cockcroft@physics.mcmaster.ca, harris@physics.mcmaster.ca
[2] Institute for Astronomy, University of Edinburgh, Blackford Hill, Edinburgh EH9 3HJ, UK; ferguson@roe.ac.uk
[3] H. H. Wills Physics Laboratory, Tyndall Avenue, Bristol BS8 1TL, UK; Avon.Huxor@bristol.ac.uk
[4] Observatoire Astronomique, Universit de Strasbourg, CNRS, 11, rue de l'Universit, F-67000 Strasbourg, France; ibata@astro.u-strasbg.fr
[5] Institute of Astronomy, University of Cambridge, Madingley Road, Cambridge CB3 0HA, UK; mike@ast.cam.ac.uk, schapman@ast.cam.ac.uk
[6] NRC Herzberg Institute of Astrophysics, 5071 West Saanich Road, Victoria, British Columbia V9E 2E7, Canada; alan.mcconnachie@nrc-cnrc.gc.ca
[7] Department of Physics and Astronomy, University of British Columbia, 6224 Agricultural Road, Vancouver, British Columbia V6T 1Z1, Canada; kwoodley@phas.ubc.ca
[8] Sydney Institute for Astronomy, School of Physics, University of Sydney, NSW 2006, Australia; gfl@physics.usyd.edu.au
[9] Department of Astronomy and Astrophysics, Pontificia Universidad Catlica de Chile, Avenue Vicuna Mackenna 4860, 7820436 Macul, Santiago, Chile; tpuzia@gmail.com
Received 2010 December 9; accepted 2011 January 12; published 2011 March 10

ABSTRACT

We use CFHT/MegaCam data to search for outer halo star clusters in M33 as part of the Pan-Andromeda Archaeological Survey. This work extends previous studies out to a projected radius of 50 kpc and covers over 40 deg^2. We find only one new unambiguous star cluster in addition to the five previously known in the M33 outer halo (10 kpc $\leqslant r \leqslant$ 50 kpc). Although we identify 2440 cluster candidates of various degrees of confidence from our objective image search procedure, almost all of these are likely background contaminants, mostly faint unresolved galaxies. We measure the luminosity, color, and structural parameters of the new cluster in addition to the five previously known outer halo clusters. At a projected radius of 22 kpc, the new cluster is slightly smaller, fainter, and redder than all but one of the other outer halo clusters, and has $g' \approx 19.9$, $(g' - i') \approx 0.6$, concentration parameter $c \approx 1.0$, a core radius $r_c \approx 3.5$ pc, and a half-light radius $r_h \approx 5.5$ pc. For M33 to have so few outer halo clusters compared to M31 suggests either tidal stripping of M33's outer halo clusters by M31, or a very different, much calmer accretion history of M33.

Key words: galaxies: evolution – galaxies: halos – galaxies: individual (M33) – galaxies: spiral – galaxies: star clusters: general – Local Group

Online-only material: color figures

1. INTRODUCTION AND BACKGROUND

Globular cluster systems (GCSs) are important tracers of galaxy formation and evolution. For example, the substructure within a galactic halo reveals its merger history, and globular clusters (GCs) can be used as one tracer of such substructure (e.g., Lynden-Bell & Lynden-Bell 1995). In this paper, we look at the Triangulum Galaxy (M33) which is the third most massive galaxy within our Local Group although it is much less well studied than the Milky Way (MW), the Magellanic Clouds, or Andromeda (M31).

In addition to the well-known stream from the disrupting Sagittarius dwarf galaxy, other evidence for substructure within the MW includes the Monoceros ring, the Orphan stream, and other more subtle overdensities (e.g., Ibata et al. 1995; Newberg et al. 2002; Belokurov et al. 2006, 2007). M31's substructure is being revealed in more and more detail with large-scale structures of very low surface brightness, including several arcs, shells, and streams (Ferguson et al. 2002; Ibata et al. 2005, 2007; Kalirai et al. 2006; Richardson et al. 2008; McConnachie et al. 2009).

Subdivisions within the MW GCS have been observed (e.g., Searle & Zinn 1978; Mackey & Gilmore 2004) with evidence that at least some are the result of accretions of dwarf satellite galaxies (Bellazzini et al. 2003; Mackey & Gilmore 2004; Forbes et al. 2004). Certain clusters still appear to be associated with their accreted satellites: most prominently, clusters associated with Sagittarius (e.g., Layden & Sarajedini 2000; Newberg et al. 2003; Bellazzini et al. 2003). The most distant GC known in the MW is still AM-1, first discovered by Madore & Arp (1979) at a galactocentric distance of ≈120 kpc. In other galaxies, clusters with large galactocentric radii (≈120 kpc) reside in the M_v–r_h parameter space between Palomar-type clusters and ultra-faint dwarfs, and this overlap is now well established (e.g., Huxor et al. 2005, Gómez et al. 2006 and Belokurov et al. 2007).

Within M31, there are now over 60 known clusters with a projected radius greater than 30 kpc (Huxor et al. 2005, 2008; Martin et al. 2006; Mackey et al. 2007, 2010). Some of these distant clusters are rather unlike their MW counterparts as they are found to be both more luminous and have larger sizes (Mackey et al. 2007). Most recently it has been shown that the outer halo clusters appear to follow other substructure (streams of enhanced surface brightness), with the probability of chance alignment less than 1% (Mackey et al. 2010). Mackey et al. conclude that the majority of these clusters are accreted along with their host satellite galaxy, as first proposed by Searle & Zinn (1978).

Observations of the M33 clusters—both young and old—have been collated in the catalog by Sarajedini & Mancone (2007; SM hereafter). This catalog includes cluster identifications and data from ground-based observations (Hiltner 1960; Melnick & D'Odorico 1978; Christian & Schommer 1982, 1988; Mochejska et al. 1998), *Hubble Space Telescope* (*HST*) imaging (Chandar et al. 1999, 2001; Bedin et al. 2005; Park & Lee 2007; Sarajedini et al. 2007; Stonkutė et al. 2008; Huxor

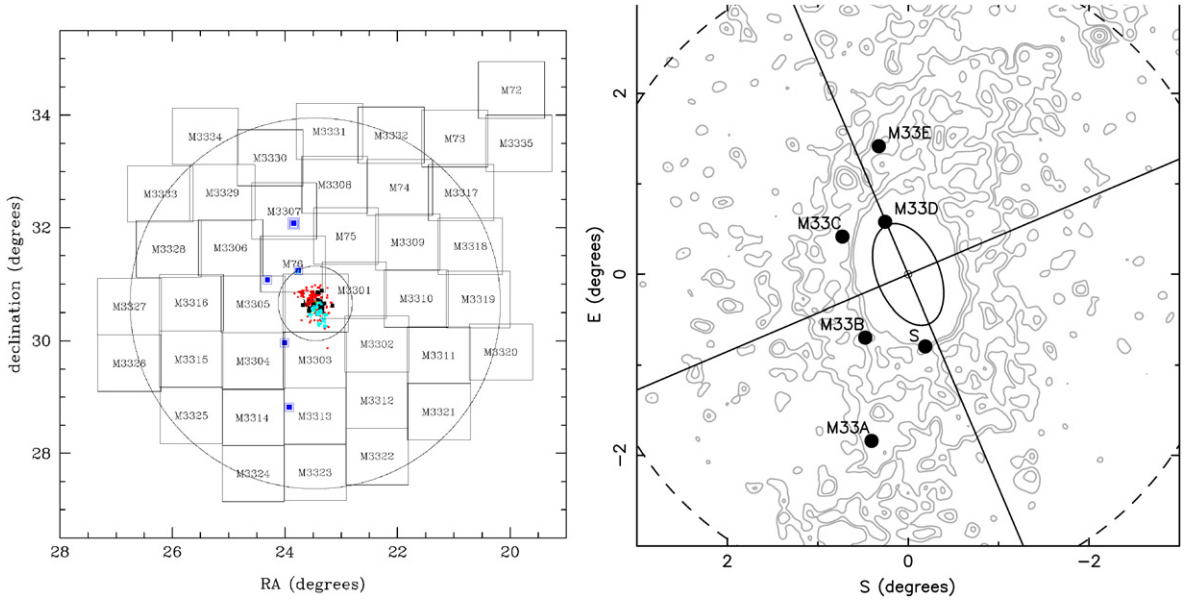

Figure 1. Left: the 41 PAndAS frames by CFHT/MegaCam around M33 used in this paper. Each square represents the 1 deg^2 field of view of MegaCam. M33c is the central field. The two circles represent projected radii of 10 kpc and 50 kpc centered on M33. Also shown are the locations of the high-confidence clusters in the Sarajedini & Mancone (2007) catalog (the outer halo cluster found by Stonkutė et al. (2008) being the only catalog's object outside the 10 kpc radius), the four outer halo clusters in Huxor et al. (2009) enclosed in one box and the newly discovered outer halo cluster enclosed in a double box. The current (2010 October) online Sarajedini & Mancone catalog is further subdivided to show the location of the 296 original clusters in red from Sarajedini & Mancone (2007) in addition to the subsequently discovered 32 clusters in black from Park & Lee (2007), 115 clusters in cyan from Zloczewski & Kaluzny (2009), and 161 (115 new) clusters in green from San Roman et al. (2009). There is much overlap between the clusters found by Zloczewski & Kaluzny (2009) and San Roman et al. (2009). Right: the outer halo clusters overlaid on the substructure map from Figure 13 in McConnachie et al. (2010).

(A color version of this figure is available in the online journal.)

et al. 2009; San Roman et al. 2009), and further data on identified clusters from Ma et al. (2001, 2002a, 2002b, 2002c, 2004a, 2004b). The SM catalog contains 595 objects of which 428 are classified as high-confidence clusters (based on *HST* and high-resolution ground-based imaging). The most recent work, currently not within the SM catalog, includes work based on CFHT/MegaCam imaging by Zloczewski et al. (2008) and San Roman et al. (2010) and *HST* imaging by Zloczewski & Kaluzny (2009), that contain 3554, 599, and 91 new star cluster candidates, respectively. (All of these M33 studies cover only the inner 1 deg^2.) Zloczewski & Kaluzny (2009) claim that ≈20% of the 3554 cluster candidates identified in Zloczewski et al. (2008) are likely to be genuine clusters. Unlike the GCSs of the MW and M31, M33 is host to intermediate-age clusters (Sarajedini et al. 1998; Chandar et al. 2002), suggesting that the evolution of M33 was different from that of both the MW and M31.

Studying the Local Group gives us the best chance to observe the remnants of galaxy formation in detail, but M33 remains to be scrutinized in as much detail as either of its larger neighboring galaxies, or the Magellanic Clouds. The work on the M33 GCS has so far been constrained to the classical disk regions, with the exception of the four outer halo clusters found by Huxor et al. (2009) between projected radii of 9.6 and 28.5 kpc and one cluster by Stonkutė et al. (2008) at a projected radius of 12.5 kpc. The outer halo clusters are important, not least because the most distant clusters may be the last that were accreted (e.g., Mackey & van den Bergh 2005). Mackey et al. (2010) have shown that M31's outer halo is rich with clusters. Huxor et al. (2009) undertook a search for M33 outer halo clusters through 12 deg^2 of the Isaac Newton Telescope Wide-Field Camera data reaching to $V \sim 24.5$ and $i \sim 23.5$. The PAndAS data allow this search to be extended to larger radii, deeper depths, and better image quality. This is the project that we undertake in this paper. We define outer halo clusters to be those which are projected beyond the isophotal radius of M33 (∼9 kpc; R. Cockcroft et al. 2011, in preparation). Such objects are sufficiently remote that they are unlikely to be associated with the main disk component of the galaxy: McConnachie et al. (2010) find little evidence from direct stellar photometry that the disk extends beyond that point. For comparison, the isophotal radius of NGC 253, an Sc-type galaxy of similar size, is $r \sim 9.8$ kpc (Jarrett et al. 2003). Ultimately however, we will require metallicity and velocity measurements to determine more definitely whether these clusters belong dynamically to the disk or halo.

2. OBSERVATIONS, DATA REDUCTION, AND CALIBRATION

We use 41 images each in g' and i' that are part of the Pan-Andromeda Archaeological Survey (PAndAS; McConnachie et al. 2009) and were taken with the Canada–France–Hawaii Telescope (CFHT)/MegaCam which has a 1 deg^2 field of view. PAndAS includes over 300 deg^2, covering a region of sky that extends to a projected radius of 150 and 50 kpc around the Andromeda (M31) and Triangulum (M33) Galaxies, respectively.

Each of the 82 processed fields, themselves a stack of four or five raw images, is labeled according to the notation shown in Figure 1. Fields M72 to M76, the five located along a line toward M31, were taken first (Ibata et al. 2007); we note that for these, CCD chip 4 was only working for M72, but not M73 to M76. The other fields M3301 to M3335 were taken in subsequent runs. The central image (called M33c) was a composite of CADC archived images prepared by Ibata et al. (2007).

All M33 images were taken with subarcsecond seeing in both g' and i'. The average seeing on g' frames was 0.″75 (standard deviation of 0.″11) and 0.″66 on i' (standard deviation of 0.″13). Images have a resolution of 0.″187 pixel^{-1}, and limiting magnitudes of $g' \approx 25.5$, $i' \approx 24.5$ (AB magnitudes on the SDSS scale) at an S/N = 10. These data were previously presented in McConnachie et al. (2010) who studied the stellar structure of the outer regions of M33 and found a large substructure, shown in Figure 1. The data were pre-processed with Elixir[10] by the CFHT team, and then reduced at the Cambridge Astronomical Survey Unit through a pipeline adapted for MegaCam images (Irwin & Lewis 2001).

3. CLUSTER SEARCH METHODS

We used two distinct methods to search for clusters within the M33 images: an automatic search and a separate follow-up visual inspection. In both cases, we started with searching the images that form an annulus in the middle of the frames around M33 (i.e., frames M3306 to M3316, including M74), followed by the images outside this annulus and finally the innermost frames. We chose this order so that we started in regions where the crowding was low but evidence for clusters existed (e.g., Huxor et al. 2009), leaving the innermost crowded fields until last. We identified and marked all the confirmed clusters in the Sarajedini & Mancone (2007) catalog on the PAndAS images, to gain experience of their appearance.

3.1. Automatic Search

We used Source Extractor (SE; Bertin & Arnouts 1996) to identify all objects in both g' and i' frames. Some values within the configuration files were changed to optimize finding clusters while cutting out as much contamination as possible (see Table 1). We then converted from a chip-oriented pixel coordinate system to a world coordinate system for each object, using the IRAF/wcsctran routine, before matching the objects across the g' and i' frames using the IRAF/xyxymatch routine. As the latter routine only outputs object coordinates, we then re-assigned all SE parameters to the matched objects, so that we could apply selection criteria using a combination of magnitude, color, half-light radius, and ellipticity as measured by SE to pick out the cluster candidates. After numerous initial tests and iterations, we have adopted the following set of criteria:

$$10.5 \leqslant g' \leqslant 14.5, \quad (1)$$

$$-1.1 \leqslant g' - i' \leqslant -0.175 * g' + 3.4375, \quad (2)$$

$$e \leqslant 0.375, \quad (3)$$

$$3.5 \leqslant r_{\rm flux} \leqslant 16.0, \quad (4)$$

and

$$r_{\rm flux} \leqslant -2.125 * g' + 41.5, \quad (5)$$

where e is the ellipticity(1 − minor/major), g' and i' are the automatic magnitude values returned from SE,[11] and $r_{\rm flux}$ is the radius (in pixels) estimated to enclose half the flux. The cluster candidates we select satisfy *all* five of the criteria.

These selection criteria are shown in Figure 2. The boundary lines were chosen so that they included almost all of the Sarajedini & Mancone (2007) catalog confirmed clusters at the edge of the disk (in the MegaCam fields M3301 and M76), while cutting out most of the contaminating objects such as stars and background galaxies. The central field, however, provides a special challenge because of the complex structure of the background light and differential reddening. As can be seen in Figure 3, our parameter boundaries do not include every one of the Sarajedini & Mancone high confidence clusters (see Section 1) in the central field.

However, our aims here were specifically to isolate candidate clusters in the halo regions. Other types of objects (especially background galaxies) populate all areas of the three parametric diagrams in Figures 2 and 3, and after many iterations we adopted the boundary lines shown as a compromise between excluding contaminants and including real clusters. Nevertheless, the unavoidable fact is that our survey area is so large (more than 40 deg^2 around M33) that even our most careful objective search criteria leave a very large number of field contaminants, which dominate the numbers of objects found in the range of magnitudes, colors, and sizes that we are looking for.

We produced a small thumbnail display region to identify each object selected by the above criteria. These regions were then displayed in the g' frame. Each object within these regions was then inspected visually and classified following the description in Section 3.2 with 1 (high confidence cluster), 2 (possible cluster), 3 (background galaxy), 4 (unknown object), or 5 (stellar object). Examples of objects in the categories 1, 2, and 3 are shown in Figure 4.

3.2. Visual Inspection

The next stage in our classification procedure was, following Section 3.1, to inspect all objects that had *not* already been selected by the automated criteria, i.e., we looked at all SE detections that did not fall within the selection boxes shown in Figure 2. This was similar to the method employed by Huxor et al. (2008, 2009). Only i' frames were inspected this way; red-giant branch stars are brighter in i' than in g' and so clusters, and RGB stars in their halo, would appear more obvious by their resolution into stars (no background galaxies would be resolved into individual stars). By also conducting a visual search in addition to the search via the selection criteria, we ensured that any obvious cluster or candidate cluster would not be overlooked, and also ensured that all g' and i' frames will have been inspected.

The easiest objects to classify were the obvious clusters and background galaxies. Clearly resolved clusters appeared as having a circular or slightly elliptical core, with uneven contours and resolved stars around the central core. Less obvious were group 1 objects which had slightly uneven contours. The least obvious candidates, group 2 objects, were the compact objects that could be clusters or galaxies, and as a result the numbers of "possible clusters" were the greatest especially in the central regions. As the contrast and scaling were changed, some objects smoothly grew, some were a faint smear with no sharp edges, and others could be seen to display spiral shape. If the object had smooth contours and if it was in a group of other objects that were clearly galaxies, the object was likely to be a galaxy and not a star cluster. Group 4 objects did not look like a cluster, a cluster candidate, a galaxy, or a star.

[10] http://www.cfht.hawaii.edu/Instruments/Imaging/MegaPrime/dataprocessing.html

[11] The following are approximate conversions between true color-corrected magnitudes and SE automatic magnitudes: $g'_{\rm true} = g'_{\rm SE} + 6.2$ and $i'_{\rm true} = i'_{\rm SE} + 6.4$.

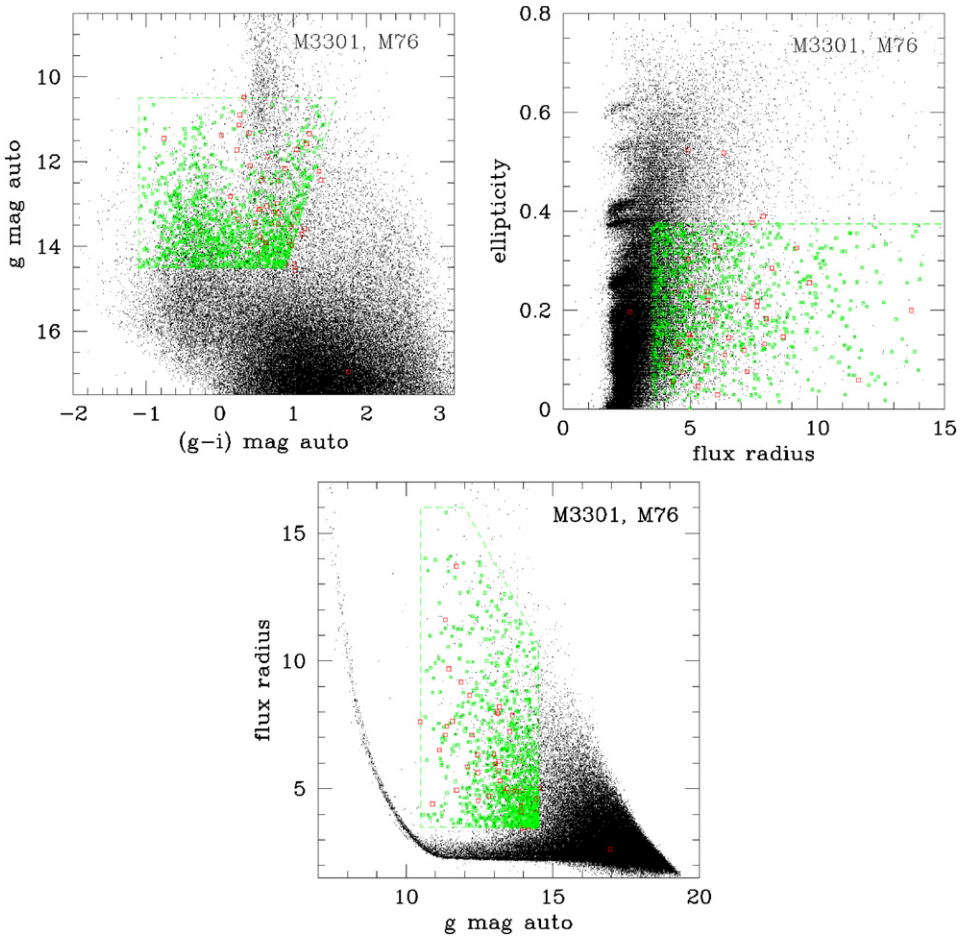

Figure 2. Two halo fields and objects on which Section 3.1's selection criteria were based. The black dots are the objects of all kinds detected by SE. The green dashed lines show the boundaries of the selection criteria (Equations (1)–(5)), and the green squares enclose those points which were picked out by all five of the selection criteria. The red squares show the high-confidence clusters in the Sarajedini & Mancone (2007) catalog. The following are approximate conversions between true color-corrected magnitudes and SE automatic magnitudes: $g'_{\rm true} = g'_{\rm SE} + 6.2$ and $i'_{\rm true} = i'_{\rm SE} + 6.4$.

(A color version of this figure is available in the online journal.)

As noted above, the influence of background contamination by galaxies on this selection process should not be underestimated. In essence, this is a needles-in-a-haystack process where we are attempting to find a small number of clusters in a huge population of contaminants, and even though our selection and culling is rigorous, there remain a large number of objects whose nature is ambiguous from the current data. Higher resolution imaging, imaging in the near-infrared where the cluster red giants would be better resolved (and which also can have better seeing), or ultimately spectroscopy, will be required for more definitive elimination of the last contaminants.

4. RESULTS

There was only one definite new outer halo cluster discovered in our study at a projected radius of 87″ (or 22 kpc, assuming a distance to M33 of 870 kpc). It was found using the automated search. The new cluster is named M33E following the naming convention begun in Huxor et al. (2009). Four of the five previously known outer halo clusters (Stonkutė et al. 2008; Huxor et al. 2009) were easily recovered. Cluster D was identified but was too compact to have been recovered without prior knowledge. Clusters A to E and S are shown in Figure 5, where S is the cluster found by Stonkutė et al. (2008).

There were 2440 candidates spread throughout the M33 halo; that is, in the region outside of the central MegaCam image. Eighty-seven (5) highest-confidence cluster candidates and 2294 (54) possible clusters were found by the automated (visual) search method.

The numbers of all classified objects from both the automated and visual inspection searches are shown in Table 2. Results of the above searches were plotted within the original selection criteria and are shown in Figure 6. We wanted to exclude the maximum amount of parameter space so that we could increase the efficiency of the automated search, and it is not obvious from this figure that more space could have been excluded. Radial density plots for the categories 1 (high confidence cluster), 2 (possible cluster), and 3 (background galaxy) are also shown in Figure 7. We compared these number densities at large radii to control fields, also taken with MegaCam and with very similar image quality, from the M31 outer halo and the field near the Draco dwarf spheroidal. The M31 fields are 2 deg^2 fields selected directly from the PAndAS data, at a similar Galactic latitude to M33 of −31.°33, at the edge of the PAndAS footprint around M31 (i.e., at a projected radius of ∼150 kpc) and did not contain any clusters—either previously known clusters, or clusters detected in the PAndAS images. The Draco fields are 7 deg^2 fields at a Galactic latitude of 34.°72 (Ségall et al. 2007).

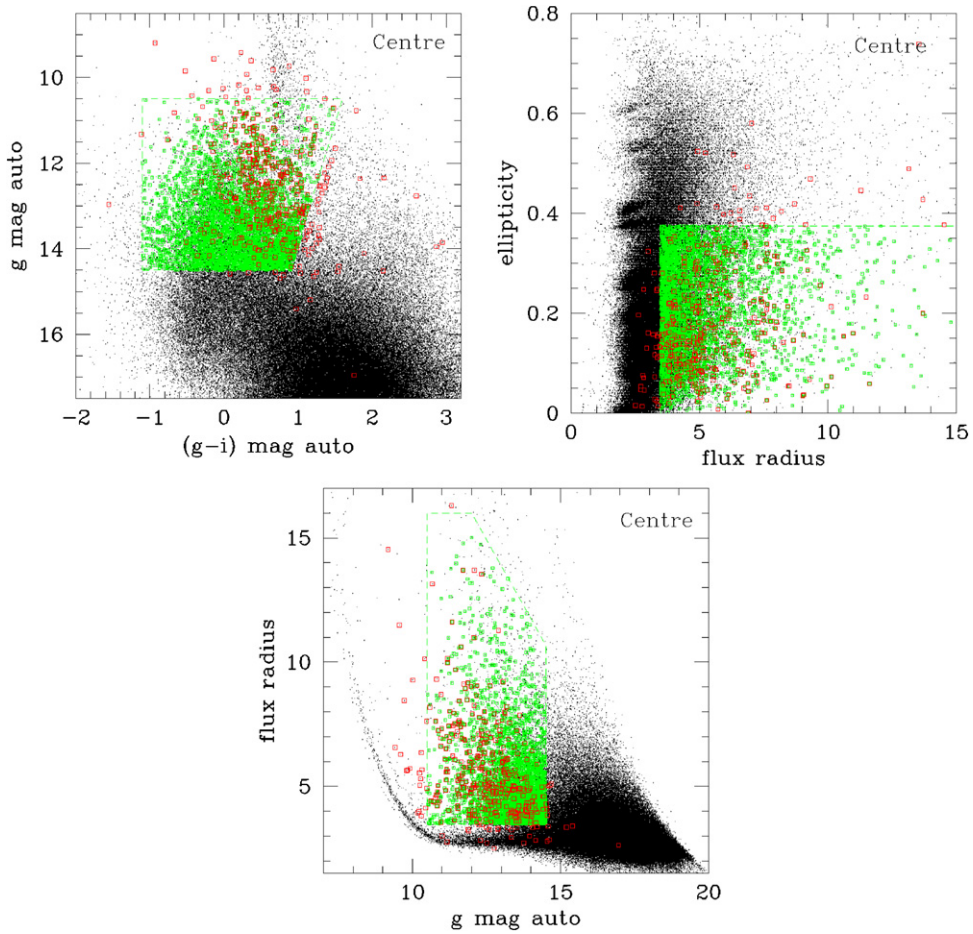

Figure 3. Objects within the central field. As with Figure 2, the black dots show the SE detections. The green dashed lines show the selection criteria, and the green squares enclose those points which were picked out by all five of the selection criteria. The red squares show the high-confidence clusters in the Sarajedini & Mancone (2007) catalog. The following are approximate conversions between true color-corrected magnitudes and SE automatic magnitudes: $g'_{\rm true} = g'_{\rm SE} + 6.2$ and $i'_{\rm true} = i'_{\rm SE} + 6.4$.

(A color version of this figure is available in the online journal.)

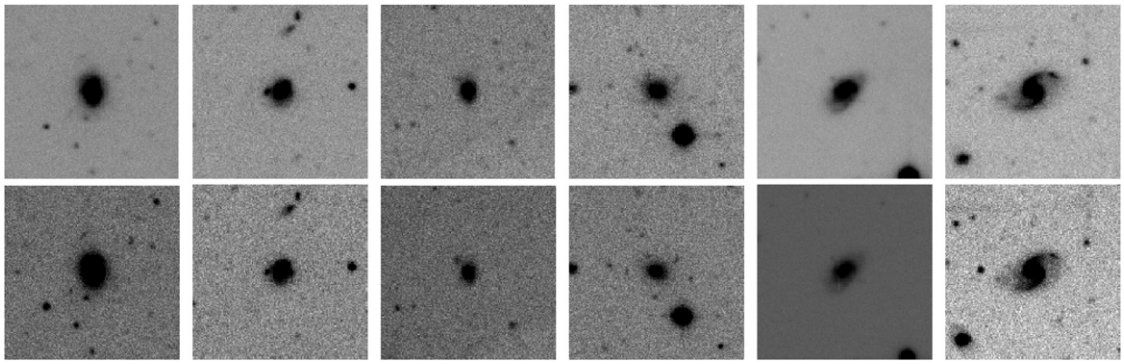

Figure 4. Six examples of classified objects in g' (top row) and i' (bottom). From left to right: two examples each of 1 (high-confidence clusters), 2 (possible cluster candidates), and 3 (galaxies). More detail is apparent when changing the scale and contrast in a DS9 window. Each box is $20''$ square, corresponding to about 84 pc square (at 870 kpc).

Our searches were again applied to the control fields following exactly the same selection criteria, and we obtained an average density of each category of objects in the control fields. The radial distribution plots indicate that few if any of the category 3 objects are genuine clusters since they show little detectable central concentration to the galaxy outside the crowded disk region. For all three categories plotted, the number density settles down to a virtually constant level similar to that of the M31 control fields for $r \gtrsim 1^\circ$, consistent with the conclusion that there are few clusters left to be found in the M33 halo down to the PAndAS limiting magnitudes. (The number density of all objects in the Draco fields is much lower than that in either the M33 or M31 fields, highlighting that it was appropriate to compare M33 with the M31 control fields.) If we count the number of candidates for the combined objects of classes 1 and 2 in Figure 7 for $r \geqslant 10$ kpc, and then subtract off the M31 background, we are left with approximately 210 ± 130 candidates (the error is estimated using the error on the M31

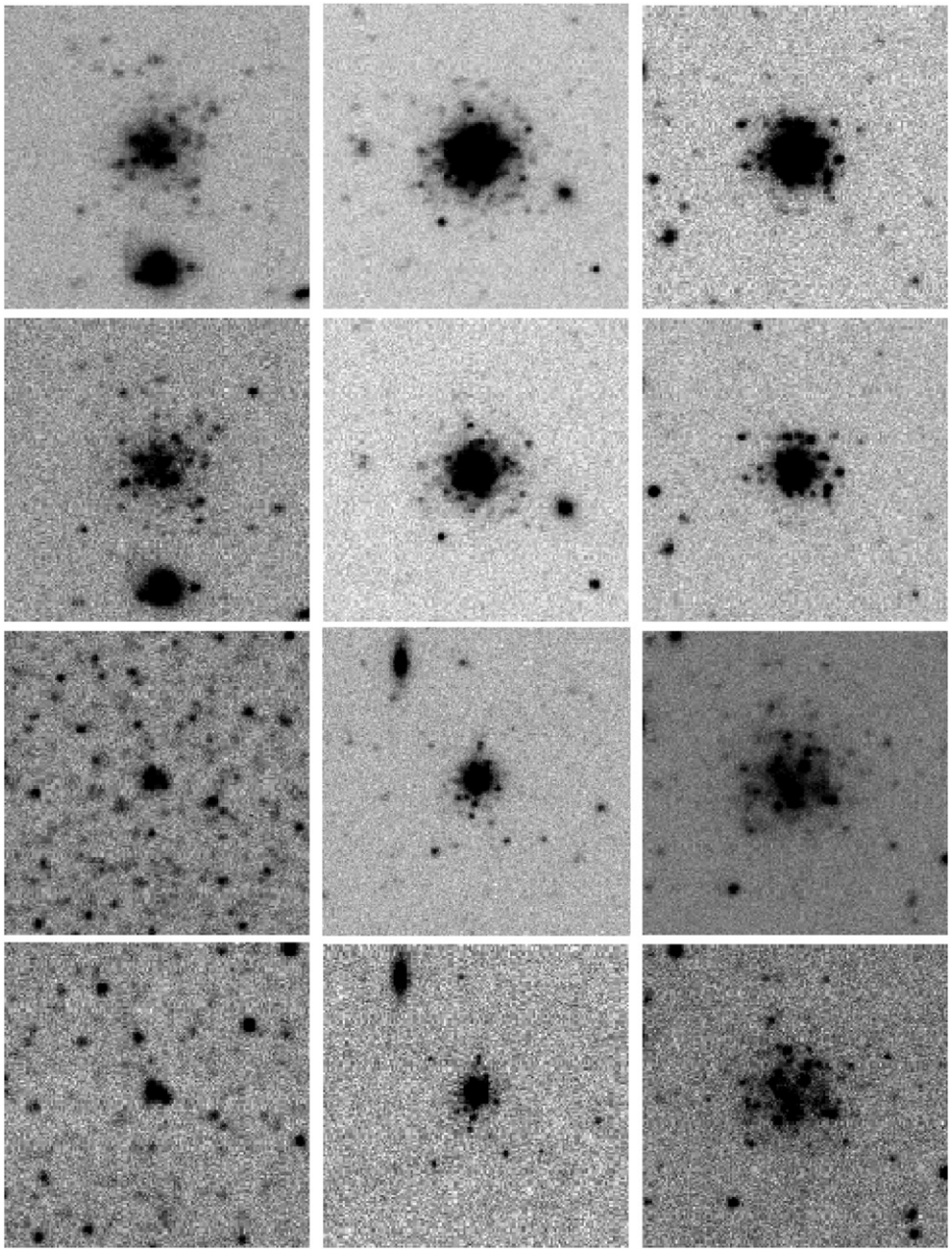

Figure 5. M33 A, B, C, D, E, and S (left to right) in g' (top) and i' (bottom). Each box is 20″ square, corresponding to about 84 pc square (at 870 kpc).

background). This number is simply an estimate of the outer halo clusters that possibly remain to be discovered, using the data we have in hand. Two hundred and ten clusters would be a generous upper limit, given the field contamination issues that we discuss.

We next measured the g' and i' magnitudes, and the colors of the six outer halo clusters. The results are shown in Table 3. For clusters A, B, C, and S we use an aperture radius of 40 pixels (7.″5) and a sky annulus between 60 and 80 pixels (11.″2–15.″0); for the smaller clusters we used 20 pixels (3.″7) with a sky annulus between 20 and 40 pixels (3.″7–7.″5) for D, and 30 pixels (5.″6) with a sky annulus between 50 and 70 pixels (9.″4–13.″1) for E. We assume an extinction correction of 0.16 in g', 0.09 in i', 0.14 in V, and 0.08 in I (Schlegel et al. 1998), and a distance of 870 kpc to M33, consistent with SM07 and Huxor et al. (2009), and corresponding to a distance modulus of $(m - M)_0 = 24.69$. We note that there is some disagreement in the literature regarding the distance to M33; see references in McConnachie et al. (2010). For the magnitude and color conversions from (g', i') to (V, I) we used

$$V = g - (0.587 \pm 0.022)(g - r) - (0.011 \pm 0.013) \quad (6)$$

and

$$I = i - (0.337 \pm 0.191)(r - i) - (0.370 \pm 0.041) \quad (7)$$

from Chonis & Gaskell (2008), and

$$(r - i)_0 = 0.37(g - r)_0 + 0.006 \quad (8)$$

from Bilir et al. (2008).

Comparing the magnitudes and colors that we measure in this paper with those in Huxor et al. (2009) for clusters A, B, C, and D, we find differences of $V_0 \leqslant 0.3$ mag and $(V - I)_0 \leqslant 0.1$ mag.

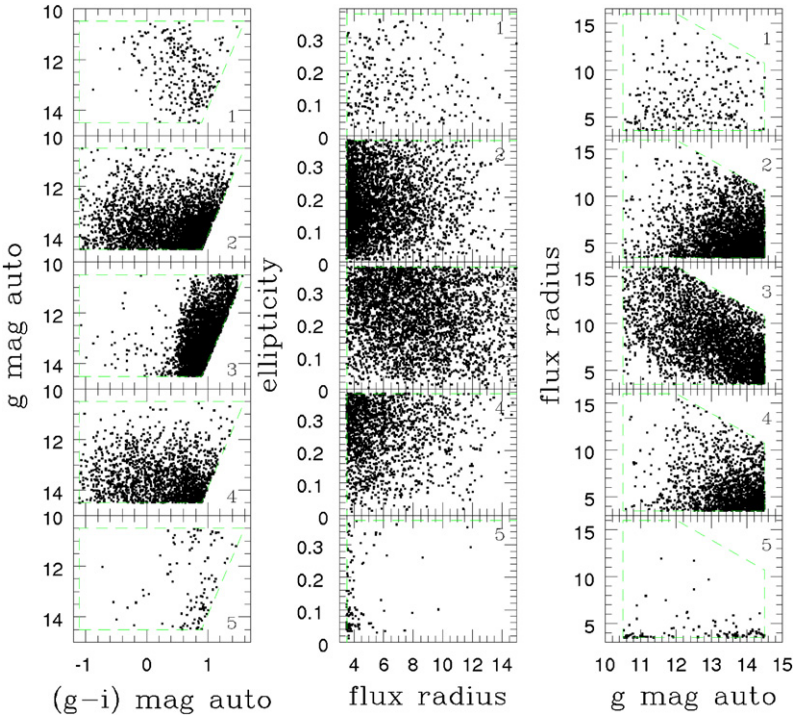

Figure 6. Classified objects after visual inspection shown in relation to the automatic selection criteria of Section 3.1. Class 1 represents high confidence candidates, class 2 are possible clusters, class 3 are background galaxies, class 4 are unknown objects, and class 5 are stellar objects. To calibrate the "mag auto" values, we added the zero-point term and corrected for airmass and color.

(A color version of this figure is available in the online journal.)

For cluster S, Stonkutė et al. (2008) measures a V magnitude of 18.5 (at $\sim 2r_h$, which roughly corresponds to our annulus size). As we measure $V_0 \sim 18.5$, the difference between our measurements is the extinction value of 0.14.

Our crude estimate for the cluster magnitude limit is currently $g'_{\rm lim} \approx 20$ ($M_g \approx -4.8$). We will quantify this more accurately in an upcoming paper by inserting fake clusters and testing recovery rates using our search methods. Although our current search limit is comfortably faint, there are small numbers of still less luminous clusters known to exist in the MW, for example (the faintest, sparse Palomar-type objects; see Figure 9). We can therefore place no quantitative limits on the numbers of such objects yet to be found in M33. Note that cluster D (Huxor et al. 2009) is a magnitude fainter than our estimated limit, but was found with *HST* imaging. We would not expect to recover such a cluster independently with the MegaCam data.

Finally, we measured the structural parameters of all six outer clusters, including the concentration parameter, and core, half-light and tidal radii. We use the GRIDFIT code described by McLaughlin et al. (2008), which fits various King-type cluster models convolved with the measured point spread function (PSF) to each object. Here we attempt to fit King (1962, 1966) and Wilson (1975) models to each object. We also use the KFIT2D code of Larsen et al. (2002) with the King (1966) model as an independent measure. The results of all fits are shown in Table 4, and examples of the fits are shown in Figures 8. We also include an independent measurement of the half-light radii using the curve of growth of the clusters ($r_{\rm ap}$). For A and D, not all of the three models converged to successful fits, but the other four clusters gave high consistency among themselves for their radii. Fitting models to cluster A was not successful because of its diffuse nature, while cluster D was extremely small. We also note that cluster S has an unusual feature in its surface profile; Stonkutė et al. (2008) also note that this cluster is asymmetrical in its inner regions. Comparing our measured structural parameters for cluster S with those from Stonkutė et al. (2008) we similarly find that this cluster has a very large core radius, although we measure slightly smaller quantities for each radius—even adjusting the value for our assumptions for the distance to M33.

Table 1
Source Extractor Values Used on the MegaCam Images

Parameter	Default Value	New Value
DETECT_MINAREA	5	4
THRESH_TYPE	...	Relative
DETECT_THRESH	1.5	5
DEBLEND_NTHRESH	32	8
CLEAN_PARAM	1.0	1.5
PHOT_APERTURES	5	3
PHOT_AUTOPARAMS	2.5,3.5	2.0,2.5
PHOT_PETROPARAMS	2.0,3.5	2.0,2.5
PHOT_FLUXFRAC	...	0.5
SATUR_LEVEL	50000	60000
MAG_ZEROPOINT	0.0	$g' = 26.7, i' = 25.98$
BACKPHOTO_TYPE	Global	Local

In Figure 9, we show the locations of all six M33 halo clusters in luminosity versus r_h, compared with the MW GCs. All clusters have low concentrations, similar to the Palomar outer halo clusters in the MW. Their half-light radii range from 4 to 20 pc, all larger than the typical mean $r_h \sim 3$ pc for the standard MW clusters, but placing them in a similar range as many of the outer halo MW clusters. A full comparison of all M33 clusters will be done in a future paper.

5. DISCUSSION AND CONCLUSIONS

We search more than 40 deg^2 of the halo of M33 with CFHT/MegaCam data for outer halo clusters using both an automated

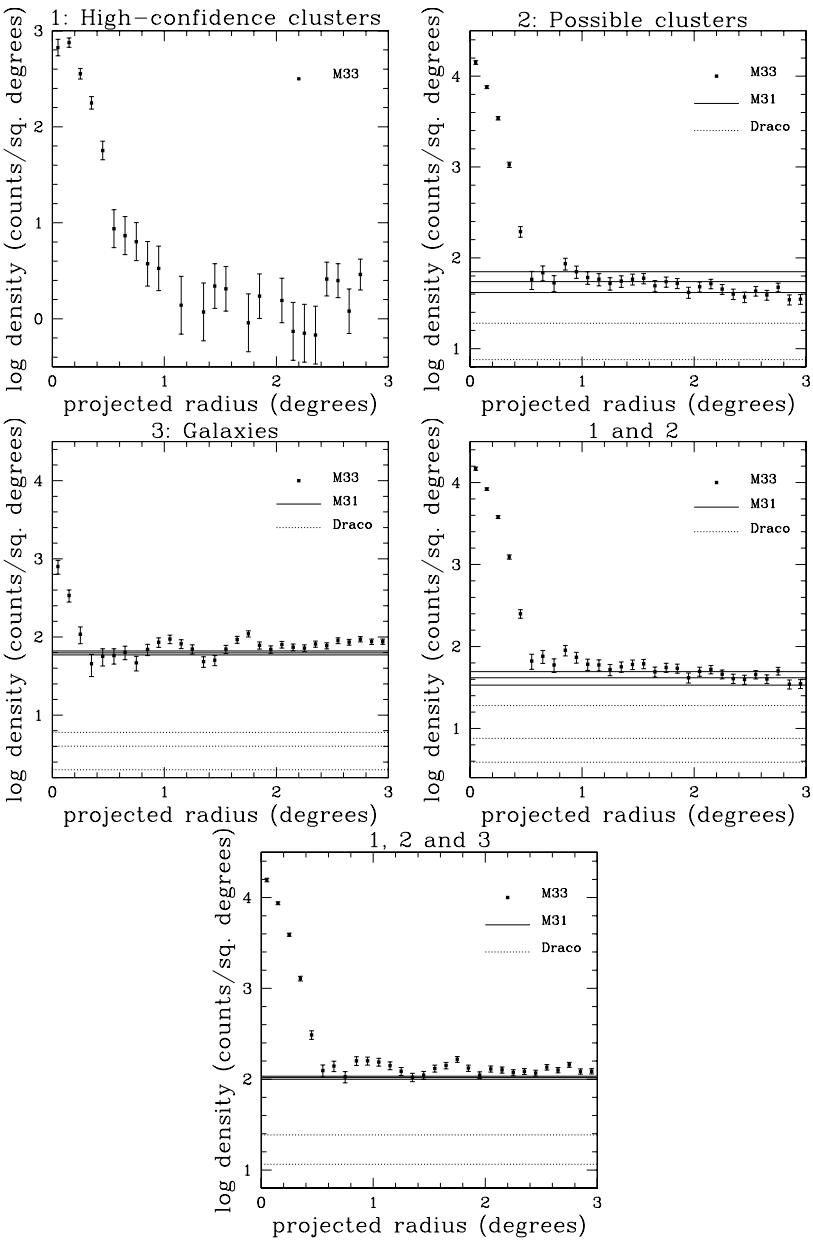

Figure 7. Radial densities of objects in circular annuli from categories 1 (high-confidence clusters), 2 (possible clusters), and 3 (background galaxies) along the top, and the sum of 1 and 2, and also 1, 2, and 3 on the bottom. Error bars on the points are simple $n^{1/2}$ uncertainties. Also shown are the mean and 1σ errors of the same categories of objects in control fields from the M31 outer halo (solid line) and Draco (dashed line). The Draco number densities are so low, as mentioned in Section 4, that in two cases the 1σ errors are larger than the mean and so cannot be plotted on a log scale. In these cases, only the mean and upper 1σ error are shown.

search and visual inspection. Unexpectedly, we find only one new cluster, which is smaller, fainter, and slightly redder than the three INT clusters found by Huxor et al. (2009) and the cluster found by Stonkutė et al. (2008). However, it does lie within the INT area of Huxor et al. (2009) but the object was not previously recognized due to its small size and faint luminosity. At a projected radius of 22 kpc, the new cluster has $g' \approx 19.9$, $(g' - i') \approx 0.6$, concentration parameter $c \approx 1.0$, a core radius $r_c \approx 3.5$ pc, and a half-light radius $r_h \approx 5.5$ pc. Its projected location is close to the feature observed in the stellar substructure (see Figure 1 and McConnachie et al. 2010). Huxor et al. (2009) note that the mean color of the previously known outer halo clusters is slightly redder ($(V - I)_0 = 0.88 \pm 0.05$ mag) than the inner clusters ($(V - I)_0 = 0.67 \pm 0.30$ mag). Our new cluster is redder still by ∼0.2 mag.

M33 has only six definite outer halo clusters between projected radii of 9 kpc $\leqslant r \leqslant$ 50 kpc and to $g'_{\rm lim} \approx 20$. We also find 2440 cluster candidates of various degrees of confidence, and although the vast majority are likely to be background contaminants, at least some of the ∼90 highest-confidence candidate objects beyond the M33 disk may be faint but genuine clusters. We cannot yet assume all the highest-confidence candidate objects are clusters without further confirmation. We will use IR data (now being acquired) and structural parameters in an upcoming paper to determine this more securely.

How many clusters could we expect to find in M33? M31 has 67 outer halo clusters already discovered, 61 of which lie in the PAndAS footprint that has been analyzed so far. These clusters have comparable luminosity to the M33 outer halo clusters and are located at projected radius 30 kpc $\leqslant r \leqslant$ 130 kpc (Mackey

Table 2
Categorized Objects in M33 PAndAS Frames

Frame	SM1	OH	1	2	3	4	5
M3301	34	...	7(3)	354(16)	106	114	0
M3302	...	...	1	69	56	8	27
M3303	1	1[a,b] + 1	3	96	43	16	8
M3304	...	1[b,c]	2	69	86	16	7
M3305	...	1[b,d]	2	83	51	19	5
M3306	...	...	2	49	92	20	0
M3307	...	1[e]	2	31	79	16	0
M3308	...	...	0	45	149	13	0
M3309	...	...	0	77	104	11	0
M3310	...	...	0	64	77	7	0
M3311	...	...	1	27	74	6	0
M3312	...	...	3	38	96	11	0
M3313	...	1[b]	2	64	60	13	0
M3314	...	...	3	44	55	13	1
M3315	...	...	2	35	87	31	0
M3316	...	...	0	56	81	14	0
M3317	...	...	1	44	114	9	0
M3318	...	...	0	25	121	5	0
M3319	...	...	0	55	96	16	0
M3320	...	...	0	29	86	6	0
M3321	...	...	0	8	74	9	0
M3322	...	...	3	26	66	11	1
M3323	...	...	0	18	69	6	1
M3324	...	...	1	63	61	16	3
M3325	...	...	0	31	61	15	3
M3326	...	...	1	29	104	15	0
M3327	...	...	0	24	81	14	3
M3328	...	...	1	32	115	14	3
M3329	...	...	5	72	81	19	6
M3330	...	...	5	67	117	15	0
M3331	...	...	2	61	127	25	0
M3332	...	...	1	58	148	22	6
M3333	...	...	3	39	129	16	2
M3334	...	...	2	35	116	15	2
M3335	...	...	2	29	87	25	0
M72	...	...	2	28	71	11	1
M73	...	...	1	45	93	13	2
M74	...	...	0	52	61	12	1
M75	...	...	0	43	95	22	0
M76	19	2[b,f]	32(8)	234(2)	54	86	3
M33c	374[g]	...	259(95)	1521(138)	84	954	19

Notes. The column headers are as follows: SM1 are the Sarajedini & Mancone (2007) catalog's confirmed clusters, OH are the outer halo clusters, 1 are our highest-confidence clusters, 2 are the possible clusters, 3 are the background galaxies, 4 are unknown objects, and 5 are stellar objects. The numbers in brackets after the highest-confidence and possible clusters indicate those candidates which matched objects in SM1.

[a] Also found in M3304.

[b] Also found by Huxor et al. (2009).

[c] Also found in M3303.

[d] Also found in M76.

[e] New cluster identified in this paper.

[f] Also found in M3305.

[g] Does not include those on frames M3301, M3303, or M76.

et al. 2010; A. Huxor et al. 2011, in preparation). Huxor et al. (2009) found a GC surface density of $\sim$0.4 deg^{-2} with their 12 deg^2 study, which they note is about half that derived for M31 over the radial range 30 kpc $\leqslant r \leqslant$ 130 kpc. Here we find an even lower GC surface density of 0.15 deg^{-2}. We note that the search in M31's outer halo is not yet complete so its GC surface density is likely to increase. M33 appears to therefore lack this type of cluster. We briefly mention two scenarios that could have resulted in this observed difference.

M33 could have had a different accretion history compared to M31—a conclusion that has been drawn before from studies of the inner regions (San Roman et al. 2010), but is now also indicated by the outer halo data. If M33 never interacted with M31 before, M33 would have had a dramatically less active accretion history.

The most compelling evidence for an accretion origin for the outer halo clusters comes from the Sagittarius dwarf in the MW (Ibata et al. 1995), and from the GCs and tidal debris streams

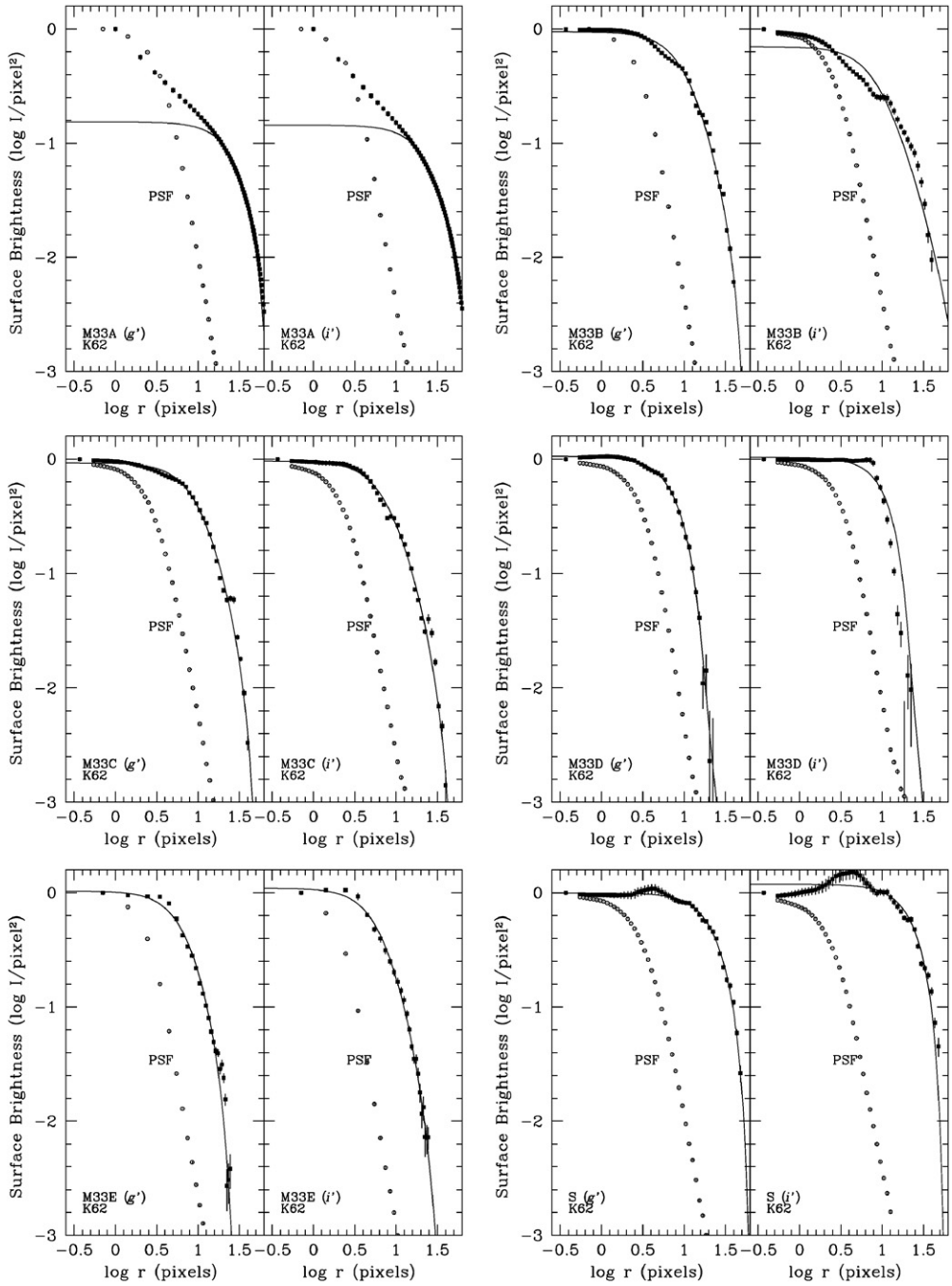

Figure 8. Examples of radial profiles for each of the six outer halo clusters. The solid points indicate the data, the line is the best fit, and the open points show the profile for the PSF. Note that for clusters A and D, the fits did not converge to a simple King-type model solution adequately.

Table 3
Outer Halo Cluster Positions, Luminosities, and Colors

Cluster	Degrees		Galactocentric Distance		g'_0	$(g'-i')_0$	V_0	$(V-I)_0$
	R.A.	Decl.	(arcmin)	(kpc)				
A	23.92388	28.82086	112	28.4	19.1	0.7	18.8	0.9
B	24.00865	29.96372	48	12.2	17.8	0.7	17.5	0.8
C	24.31026	31.07433	45	11.3	18.4	0.8	18.1	0.8
D	23.75916	31.23925	37	9.4	21.3	0.8	20.9	1.0
E	23.84466	32.07559	87	21.9	19.8	0.5	19.6	1.1
S	23.24374	29.8675	49	12.3	18.9	0.8	18.5	0.8

Note. We assume a distance of 870 kpc to M33, consistent with SM07 and Huxor et al. (2009), and that M33's center is located at ($01^h33^m50\overset{s}{.}9$, $30^d39^m37^s$).

Table 4
Outer Halo Cluster Structural Parameters, Including Concentration, c, Core Radii, Half-light Radii, and Tidal Radii, Using Both GRIDFIT and KFIT2D

Cluster	Model	Band	Seeing/FWHM	c	Radii (pc)			
					Core	Half	Tidal	r(ap)
	K62	i	3.8	0.5	16.9	20.1	68.0	11.7
A	K66	i	3.8	0.4	17.7	20.3	83.2	
	W	...	...	...	...	...	...	
	kfit2d	i	3.8	0.7	11.7	11.6	59.8	
	K62	g	4.0	0.8	6.1	9.4	44.0	9.0
B	K66	g	4.0	0.9	6.3	9.4	56	
	W	g	4.0	1.0	6.6	9.4	87.3	
	kfit2d	g	4.0	1.1	6.0	10.9	78.5	
	K62	g	4.0	0.8	5.6	8.7	40.7	7.8
C	K66	i	3.3	1.0	4.5	7.3	48.1	7.8
	W	i	3.3	1.0	4.9	7.1	70.8	
	kfit2d	i	3.3	1.3	3.8	8.8	81.9	
	K62	g	4.5	0.3	4.7	4.8	13.6	4.7
D	K66	...	...	...	...	...	...	
	W	...	...	...	...	...	...	
	kfit2d	g	4.5	0.4	4.1	3.7	9.8	
	K62	i	2.6	0.8	3.3	5.2	25.5	5.1
E	K66	i	2.6	0.9	3.5	5.2	31.4	
	W	g	3.1	1.2	3.6	5.6	65.8	5.1
	kfit2d	i	2.6	1.1	2.7	5.0	32.4	
	K62	g	4.6	0.3	15.8	15.7	42.7	18.7
S	K66	i	3.4	0.4	14.8	16.7	67.31	18.7
	W	i	3.4	0.2	15.8	19.2	121.4	
	kfit2d	i	3.4	0.7	17.9	18.7	93.7	

Notes. We report the best fit to the data, whether in g' or in i'. Also shown are half-light radii estimates (r_{ap}) using curves of growth, for an independent check on the upper limit of the half-light radii. We assume a distance of 870 kpc to M33, consistent with SM07 and Huxor et al. (2009), and corresponding to a distance modulus of $(m - M)_0 = 24.69$.

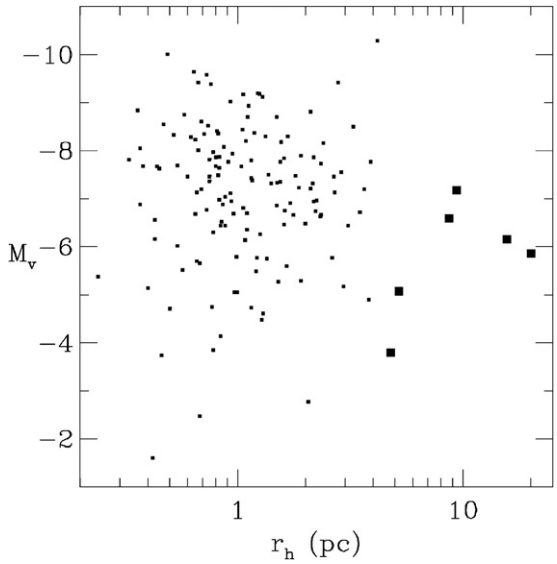

Figure 9. Absolute magnitudes vs. the half-light radius in parsecs for both the Milky Way clusters (Harris 1996), shown in small boxes, and the six M33 outer halo clusters, shown as larger boxes.

in M31 (Mackey et al. 2010), but it is still far from clear how general a result this is.

However, another exciting and more likely prospect, given the tidal distortion of M33, is that perhaps some of M33's outer halo clusters were heavily stripped off in a previous dynamical interaction with M31 (Huxor et al. 2009; San Roman et al. 2010). Some of the GCs originally belonging to M33 may now be closer to M31, but it will be difficult to disentangle the populations. A more detailed comparison will require spectroscopic studies of these clusters to determine properties that may link the divided populations. Although unlikely, some clusters may be beyond the area that we have imaged so far around M33. These scenarios are not mutually exclusive. Further discussion and comparison with the M33 halo star population will come in subsequent work now in progress.

R.C. and W.E.H. thank the Natural Sciences and Engineering Research Council of Canada for financial support. This research has made use of the NASA/IPAC Extragalactic Database (NED) which is operated by the Jet Propulsion Laboratory, California Institute of Technology, under contract with the National Aeronautics and Space Administration.

Based on observations obtained with MegaPrime/MegaCam, a joint project of CFHT and CEA/DAPNIA, at the Canada–France–Hawaii Telescope (CFHT) which is operated by the National Research Council (NRC) of Canada, the Institute National des Sciences de l'Univers of the Centre National de la Recherche Scientifique of France, and the University of Hawaii. R.C. thanks the CFHT staff for much support.

Thanks to all our collaborators in the PAndAS and to the anonymous referee for providing useful comments that improved this paper. R.C. also thanks the Universities of Edinburgh and Cambridge for funding collaborative visits.

REFERENCES

Bedin, L. R., Piotto, G., Baume, G., Momany, Y., Carraro, G., Anderson, J., Messineo, M., & Ortolani, S. 2005, A&A, 444, 831
Bellazzini, M., Ferraro, F. R., & Ibata, R. 2003, AJ, 125, 188
Belokurov, V., et al. 2006, ApJ, 642, L137
Belokurov, V., et al. 2007, ApJ, 658, 337
Bertin, E., & Arnouts, S. 1996, A&AS, 117, 393
Bilir, S., Ak, S., Karaali, S., Cabrera-Lavers, A., Chonis, T. S., & Gaskell, C. M. 2008, MNRAS, 384, 1178
Chandar, R., Bianchi, L., & Ford, H. C. 1999, ApJS, 122, 431
Chandar, R., Bianchi, L., & Ford, H. C. 2001, A&A, 366, 498
Chandar, R., Bianchi, L., Ford, H. C., & Sarajedini, A. 2002, ApJ, 564, 712
Chonis, T. S., & Gaskell, C. M. 2008, AJ, 135, 264
Christian, C. A., & Schommer, R. A. 1982, ApJS, 49, 405
Christian, C. A., & Schommer, R. A. 1988, AJ, 95, 704
Ferguson, A. M. N., Irwin, M. J., Ibata, R. A., Lewis, G. F., & Tanvir, N. R. 2002, AJ, 124, 1452
Forbes, D. A., Strader, J., & Brodie, J. P. 2004, AJ, 127, 3394
Gómez, M., Geisler, D., Harris, W. E., Richtler, T., Harris, G. L. H., & Woodley, K. A. 2006, A&A, 447, 877
Harris, W. E. 1996, AJ, 112, 1487
Hiltner, W. A. 1960, ApJ, 131, 163
Huxor, A. P., Ferguson, A. M. N., Barker, M. K., Tanvir, N. R., Irwin, M. J., Chapman, S. C., Ibata, R., & Lewis, G. 2009, ApJ, 698, L77
Huxor, A. P., Tanvir, N. R., Ferguson, A. M. N., Irwin, M. J., Ibata, R., Bridges, T., & Lewis, G. F. 2008, MNRAS, 385, 1989
Huxor, A. P., Tanvir, N. R., Irwin, M. J., Ibata, R., Collett, J. L., Ferguson, A. M. N., Bridges, T., & Lewis, G. F. 2005, MNRAS, 360, 1007
Ibata, R. A., Chapman, S., Ferguson, A. M. N., Lewis, G., Irwin, M., & Tanvir, N. 2005, ApJ, 634, 287
Ibata, R. A., Gilmore, G., & Irwin, M. J. 1995, MNRAS, 277, 781
Ibata, R. A., Martin, N. F., Irwin, M., Chapman, S., Ferguson, A. M. N., Lewis, G. F., & McConnachie, A. W. 2007, ApJ, 671, 1591
Irwin, M., & Lewis, J. 2001, New Astron. Rev., 45, 105
Jarrett, T. H., Chester, T., Cutri, R., Schneider, S. E., & Huchra, J. P. 2003, AJ, 125, 525
Kalirai, J. S., et al. 2006, ApJ, 648, 389
King, I. R. 1962, AJ, 67, 471
King, I. R. 1966, AJ, 71, 64
Larsen, S. S., Brodie, J. P., Sarajedini, A., & Huchra, J. P. 2002, AJ, 124, 2615
Layden, A. C., & Sarajedini, A. 2000, AJ, 119, 1760
Lynden-Bell, D., & Lynden-Bell, R. M. 1995, MNRAS, 275, 429
Ma, J., Zhou, X., & Chen, J. 2004a, Chin. J. Astron. Astrophys., 4, 125
Ma, J., Zhou, X., & Chen, J. 2004b, A&A, 413, 563
Ma, J., Zhou, X., Chen, J., Wu, H., Jiang, Z., Xue, S., & Zhu, J. 2002a, Chin. J. Astron. Astrophys., 2, 197
Ma, J., Zhou, X., Chen, J., Wu, H., Jiang, Z., Xue, S., & Zhu, J. 2002b, AJ, 123, 3141
Ma, J., Zhou, X., Chen, J., Wu, H., Kong, X., Jiang, Z., Zhu, J., & Xue, S. 2002c, Acta Astron., 52, 453
Ma, J., Zhou, X., Kong, X., Wu, H., Chen, J., Jiang, Z., Zhu, J., & Xue, S. 2001, AJ, 122, 1796
Mackey, A. D., & Gilmore, G. F. 2004, MNRAS, 355, 504
Mackey, A. D., & van den Bergh, S. 2005, MNRAS, 360, 631
Mackey, A. D., et al. 2007, ApJ, 655, L85
Mackey, A. D., et al. 2010, ApJ, 717, L11
Madore, B. F., & Arp, H. C. 1979, ApJ, 227, L103
Martin, N. F., Ibata, R. A., Irwin, M. J., Chapman, S., Lewis, G. F., Ferguson, A. M. N., Tanvir, N., & McConnachie, A. W. 2006, MNRAS, 371, 1983
McConnachie, A. W., Ferguson, A. M. N., Irwin, M. J., Dubinski, J., Widrow, L. M., Dotter, A., Ibata, R., & Lewis, G. F. 2010, ApJ, 723, 1038
McConnachie, A. W., et al. 2009, Nature, 461, 66
McLaughlin, D. E., Barmby, P., Harris, W. E., Forbes, D. A., & Harris, G. L. H. 2008, MNRAS, 384, 563
Melnick, J., & D'Odorico, S. 1978, A&AS, 34, 249
Mochejska, B. J., Kaluzny, J., Krockenberger, M., Sasselov, D. D., & Stanek, K. Z. 1998, Acta Astron., 48, 455
Newberg, H. J., et al. 2002, ApJ, 569, 245
Newberg, H. J., et al. 2003, ApJ, 596, L191
Park, W., & Lee, M. G. 2007, AJ, 134, 2168
Richardson, J. C., et al. 2008, AJ, 135, 1998
San Roman, I., Sarajedini, A., & Aparicio, A. 2010, ApJ, 720, 1674
San Roman, I., Sarajedini, A., Garnett, D. R., & Holtzman, J. A. 2009, ApJ, 699, 839
Sarajedini, A., Barker, M. K., Geisler, D., Harding, P., & Schommer, R. 2007, AJ, 133, 290
Sarajedini, A., Geisler, D., Harding, P., & Schommer, R. 1998, ApJ, 508, L37
Sarajedini, A., & Mancone, C. L. 2007, AJ, 134, 447
Schlegel, D. J., Finkbeiner, D. P., & Davis, M. 1998, ApJ, 500, 525
Searle, L., & Zinn, R. 1978, ApJ, 225, 357
Ségall, M., Ibata, R. A., Irwin, M. J., Martin, N. F., & Chapman, S. 2007, MNRAS, 375, 831
Stonkutė, R., et al. 2008, AJ, 135, 1482
Wilson, C. P. 1975, AJ, 80, 175
Zloczewski, K., & Kaluzny, J. 2009, Acta Astron., 59, 47
Zloczewski, K., Kaluzny, J., & Hartman, J. 2008, Acta Astron., 58, 23